RESEARCH ARTICLE

High-Dimensional Multiple Fractional-Order Optimizer for Rotor Side Converter of Doubly-Fed Induction Generators

XINGHUA TAO[1], NAN MO[2], JIANBO QIN[1], XIAOZHE YANG[1], LINFEI YIN[2], AND LIKUN HU[2]

[1]School of Intelligent Manufacturing, Nanning University, Nanning, Guangxi 530000, China
[2]School of Electrical Engineering, Guangxi University, Nanning, Guangxi 530004, China

Corresponding author: Linfei Yin (yinlinfei@gxu.edu.cn)

ABSTRACT The work proposes high-dimensional multiple fractional-order optimization algorithm (HMFOA) to tune the controller parameters of the rotor side converter of doubly-fed induction generator-based wind turbines to achieve higher control performance. The case studies are verified in eight benchmark mathematical optimization problems; the results illustrate that the proposed optimizer has fast convergence speed, high computational precision, and avoidance of falling into local optimums. Compared to four other algorithms, the results show that HMFOA obtains the optimal parameters of controllers and achieves more accurate power point tracking capability and certain fault ride-through capability, which verifies the feasibility and effectiveness of the algorithm.

INDEX TERMS High dimension, fractional-order, optimization algorithm, DFIG, rotor side converter.

I. INTRODUCTION

Wind energy has a large storage capacity and is a renewable and clean energy source that has received wide attention from researchers and scholars [1], [2]. Currently, the development of wind power has become a significant force driving environmental improvement and economic transformation [3]. With the integration of the DFIG and advanced power electronics equipment [4], the generation capacity of DFIG-based wind energy systems (DFIG-WESs) is increasing [5].

The control strategy of the converter of DFIG can improve the small capacity of the excitation converter of a DFIG and the weak control ability of the DFIG, especially under non-ideal grid conditions. Three types of control are widely applied in the DFIG [6]. (1) Direct power control (DPC) directly realizes the speed regulation of DFIG by regulating power output. In the hybrid system with super capacitor, fuel cell and DFIG wind turbine, DPC was developed to control

The associate editor coordinating the review of this manuscript and approving it for publication was Engang Tian.

the DFIG wind turbine [7]. Reference [8] designs a direct torque control (DTC) method with parallel compensators to restrain active and reactive power ripple in unbalanced grid states. In summary, the DPC has large fluctuations in current, active power, and reactive power. (2) The DTC realizes rotor speed control through electromagnetic torque control. A DTC based on instantaneous flux damping has been presented to the symmetrical voltage sag of the DFIG [9]. One of the significant drawbacks of the DTC is the large fluctuations in torque and magnetic chain produced by the hysteresis loop controllers [10]. The DPC and DTC mentioned above have not been widely employed in the DFIG. (3) Vector control (VC) generally adopts two closed-loop control frameworks: an external power loop and an internal current control loop The VC was utilized to control maximum power point tracking and fault ride-through in DFIG [11]. Furthermore, an improved VC strategy based on proportional integral resonance control was proposed to control brushless DFIG [12]. To mitigate the disadvantages that some parameters (e.g., flux and torque) of the DFIG are challenging to measure, the

VC method of direct field-oriented control has been studied in [13]. Furthermore, in [14], two kinds of nonlinear control methods based on vector control were proposed for the control of DFIG and compared the stability of the two methods. The VC technology, the most widely used method in DFIG for control, is mature, strong robust, and has excellent steady-state performance; this paper employs the VC method to control DFIG under different operating states.

The DFIG control system contains two controllers [15], [16]: grid side converter (GSC) is mainly developed to stabilize DC bus voltage and not directly participate in DFIG control [17]; rotor side converter (RSC) mainly controls rotor speed and reactive power for realizing DFIG operation control [18]. This study mainly focuses on the maximum power point tracking (MPPT) of DFIG. The DFIG in three-phase coordinates is a high-order, multivariate, nonlinear, strongly coupled, complex time-varying system. To realize the effective power adjustment of RSC, the two currents need to be controlled separately to achieve the operational control of DFIG. The traditional method of tuning control parameters is the engineering adjustment method, which mainly relies on the production experience of operators to obtain the target parameters after repeated tests. To change operating conditions, the control performance of the controller may change drastically. Therefore, a more reliable and effective method should be needed to tune the controller parameters considering various operating conditions. The intelligent optimization method, which has been widely applied in the controllers, breaks away from the dependence on the accurate mathematical model of the system and shows strong support for the variation of system parameters.

Intelligent optimization algorithms are broadly divided into three main classes, evolutionary algorithms, swarm intelligence algorithms, and algorithms based on physical phenomena [19]. (1) An evolutionary algorithm is inspired by evolution and is widely employed in controller parameters tuning. A hybrid system using a conventional genetic algorithm (GA) and bacterial foraging (BF) was applied to tune proportional-integral-derivative (PID) parameters for voltage control [20]. Reference [21] applied an improved differential evolution (DE) algorithm for complex optimization problems. Besides, the biogeography-based optimization (BBO) and shuffle frog leaping algorithm have been combined to strengthen the balance between exploration and exploitation for minimum spanning tree problems [22]. (2) Swarm intelligence algorithms, which are based on biological collectives and social agents, mostly imitate the social behavior of groups of organisms in nature. In [23], the firefly algorithm was applied to minimize the low-frequency oscillation and reduce the maximum overshoot and the stability time by the parameter tuning of the power system stabilizer. Additionally, a gray wolf optimization (GWO) algorithm has been employed for multi-objective models [24]. Reference [25] combines two optimization methods to tune the parameters of automatic voltage controllers. Additionally, the moth fire optimization (MFO) algorithm was utilized in the WES to set

TABLE 1. Related study.

Reference	Method	Purpose
[7]	Adaptive direct power control	Power control for DFIG
[8]	Voltage-modulated direct power control	Power control for DFIG
[9]	New reference-generation-strategy	Direct torque control of DFIG
[11]	Novel-grouped grey wolf optimizer	Parameters for optimizing of controller of DFIG
[16]	Multivariable adaptive super-twisting approach	Maximum power point tracking control for DFIG
[17]	PID optimization algorithm	Parameters optimization problem of DFIG
[18]	Novel multi-objective PID optimization algorithm	Minimum deviation of rotor speed and reactive power for controller
[23]	Multi-objective metaheuristic Firefly algorithm	Robust tuning of excitation controller for stability enhancement
[24]	Adaptive bridging mechanism based on β-chaotic sequence	For the improvement of Grey Wolf Optimizer
[25]	New optimal controller tuning method	Controller optimization for an AVR system
[26]	Moth-Flame optimization	Optimization based blade pitch controller
[27]	Multi-objective evolutionary artificial bee colony algorithm	Optimizing network topology design
[29]	Multi-verse optimizer approach	Selecting optimal features and optimizing the parameters of SVM
[30]	Novel hybrid PSO search technique	Optimization of PID controller parameters
This study	HMFOA	Parameters for optimizing HDMFOC for DFIG

blade pitch controller parameters for enhancing the damping of output power and voltage oscillations [26]. In [27], a multi-objective optimization method based on goal programming was applied for computer topology design. Furthermore, the improved firefly algorithm, combined with a local search operator and genetic operator, has been used for electrohydrodynamic inkjet printing systems [28]. (3) The algorithm based on physical phenomena realizes the optimization by imitating physical phenomena. A multi-dimensional optimization (MVO) algorithm has been developed to support vector machine (SVM) for rectifying the main parameters of SVM and finding the optimal feature set [29]. Intelligent optimization algorithms based on physical phenomena are the algorithms that search agents communicate and travel in search scope based on physical laws [30]. No suitable intelligent algorithm can solve any optimization problems [31]. In other words, a specific intelligent algorithm used in one group of optimization problems can achieve better optimization results but may show poor performance in different groups of optimization problems.

The related optimization methods and control methods have been summarized. Optimization methods have also been summarized for the optimization of wind turbine parameters as shown in TABLE 1. Inspired by PID optimization algorithms being applied to optimize parameters in PID controllers for wind turbines, this study proposes HDMFOC controller-related optimization algorithms to optimize the controller parameters of HDMFOC.

In this study, the RSC is controlled by a VC loop formed by high-dimensional multiple fractional-order controllers

(HDMFOC). The HDMFOC can synthesize multi-layer on numerous levels and process the feedback information more accurately. From the perspective of control, feedback multi-dimensional information means that the larger the control dimension, the higher the control performance [32]. Inspired by HDMFOC [33], this work proposes a high-dimensional multiple-fractional order optimization algorithm (HMFOA) to tune HDMFOC parameters.

The HMFOA has three dimensions of search directions: proportional direction, fractional-order integral direction, and fractional-order differential direction [34]. Three directions have different exploration and exploitation abilities and can balance exploration and exploitation overall. The HMFOA contains the orders of fractional-order calculus and three different adaptive decreasing functions.

The characteristics of the HMFOA can be summarized as follows.

i) The HMFOA is inspired by the theory of HDMFOC and contains proportional operators, fractional-order integral operators, and fractional-order differential operators with three-dimensional search directions. The fractional-order integral operator could enhance exploration capability, and the fractional-order differential operator could increase exploitation capability.

ii) HMFOA introduces the orders of fractional-order integral operators and fractional-order differential operators. The HMFOA has more degrees of freedom and can expand the scope of the search.

iii) The HMFOA designs three different decreasing functions that vary adaptively with iteration times, corresponding to the proportional operator, fractional-order integral/differential operators, achieving a smooth transition from exploration to exploitation overall.

The rest of this work, including Section II describes the principle of HDMFOC and the procedures of HMFOA. The specific modeling and control framework of DFIG is described in Section III. Section IV carries out the case studies. Section IV-C demonstrates the conclusions of the paper.

II. HDMFOA

A. HDMFOC

The input information of HDMFOC has numerous dimensions (FIGURE 1), which can ensure the comprehensiveness of the information. The HDMFOC calculates the multi-level fractional order of the input information.

The HDMFOC output is

$$C_{\text{HDMFOC}}(s) = \sum_{i=1}^{\alpha_i} \sum_{j=1}^{\alpha_j} (\lambda_{j,i} \theta_j s^{\mu_{j,i}}) \tag{1}$$

where, α_i and α_j means the numbers of fractional orders and input information, respectively; $\mu_{j,i}$ and $\lambda_{j,i}$ are fractional-order coefficients. The information $\{\theta_1, \theta_2, \ldots \theta_j\}$ is linked with related fractional-order structures. In HDMFOC, a total of $2\alpha_i\alpha_j$ parameters need to be configured, i.e., $\lambda_{1,1}, \lambda_{1,2}, \ldots,$
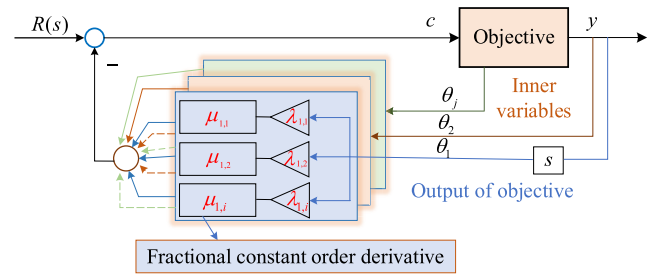
FIGURE 1. Structure block diagram of HDMFOC.

$\lambda_{1,i}, \lambda_{2,1}, \lambda_{2,2}, \ldots, \lambda_{j,i}, \mu_{1,1}, \mu_{1,2}, \ldots, \mu_{1,i}, \mu_{2,1}, \mu_{2,2}, \ldots, \mu_{j,i}$.

In (1), $s^{\mu_{j,i}}$ is the fractional order calculus. The fractional calculus of the fractional-order proportional-integral-derivative can be calculated as (2):

$$_aD_t^\alpha = \begin{cases} d^\alpha/dt^\alpha, & \mathbf{R}(\alpha) > 0 \\ \int_a^t (d\tau)^\alpha, & \mathbf{R}(\alpha) < 0 \\ 1, & \mathbf{R}(\alpha) = 0 \end{cases} \tag{2}$$

where a and t imply the low and high limits of fractional-order, respectively; α can be a complex number, means the fractional-order; and $\mathbf{R}(\alpha)$ means the real part of the variable α.

For the computation, the fractional-order operation with the Riemann-Liouville approximation can be calculated as (3):

$$_aD_t^\alpha f(t) = \frac{1}{\Gamma(n-\alpha)} \frac{d^n}{dt^n} \int_a^t (t-\tau)^{n-\alpha-1} f(\tau) d\tau \tag{3}$$

where n should be an integer, $n = [\alpha] + 1; [\alpha]$ denotes the integer part $\alpha; \Gamma(n-\alpha) = (n-\alpha-1)!$.

This study focuses on proposing an optimization algorithm. The specific research related to the control algorithm can be found in the literature [35].

B. BASIC CONCEPTS OF HMFOA

The HMFOA is inspired by the HDMFOC, which inputs multi-dimensional information and performs multi-level fractional calculus calculation.

Intelligent optimization algorithms first randomly initialize the initial set of position vectors of the population and then iterate continuously to get the new set of position vectors according to the special rules until the optimal position vectors are found [36]. Intelligent optimization algorithms perform stochastic optimization under certain rules, which can hardly guarantee the optimal solution in one iteration. The optimization process of intelligent optimization algorithms is generally divided into exploration and exploitation processes. The exploration combines random solutions with high random probability to find possible regions. As shown in FIGURE 2, x_3 and x_4 search for the global optimal solution region, the rational design of the exploration can effectively avoid falling into local optimal. The exploitation combines
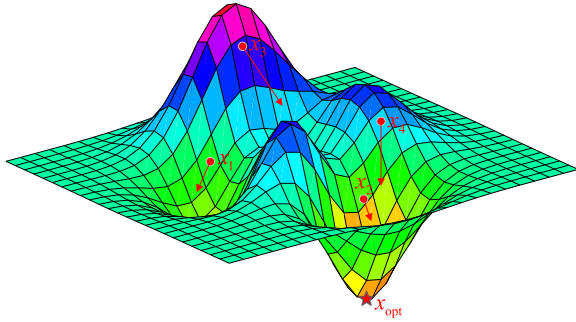
FIGURE 2. Exploration and exploitation diagram in an intelligent optimization algorithm.

FIGURE 3. Search scope of three update directions.

FIGURE 4. Optimization process in high-dimensional multiple fractional-order optimization algorithm.

stochastic solutions with low randomness to limit the search to the vicinity of the optimal local solution. The range of random solution variation during the exploitation is smaller than the exploration; the search accuracy is higher than the exploration. As shown in FIGURE 2, x_1 and x_2 search for local optimal solutions.

In HMFOA, the procedure for renewing the location of the solution follows.

$$x_i^{t+1} = x_{pi}^t + r_1 \times (k_1 \left| x_{pi}^t - x_i^t \right|) \tag{4}$$

$$x_i^{t+1} = x_{pi}^t + r_2 \times (k_2 \left| \sum_{j=0}^{t} (x_{pi}^j - x_i^j) \right|^\varphi) \tag{5}$$

$$x_i^{t+1} = x_{pi}^t + r_3 \times (k_3 \left| (x_{pi}^t - x_i^t) - (x_{pi}^{t-1} - x_i^{t-1}) \right|^\delta) \tag{6}$$

where x_i^t and x_i^{t+1} are the i-th current solutions in the t-th and $(t + 1)$-th iteration, respectively; x_{pi}^t is the i-th optimal position; $r_1/r_2/r_3$ are adaptive random numbers; k_1, k_2, and k_3 are product factors of proportional, fractional-order integral, and differential operators, respectively; φ and δ mean integral and differential operator fractional-orders, respectively; $||$ represents the absolute value.

In the general computational laws of intelligent optimization algorithms, the core of iteration rule calculation is the step-size span between the current position and the current optimal position $\left| x_{pi}^t - x_i^t \right|$. As shown in (4), the distance is adjusted by setting different random numbers. To further expand the exploration ability and enhance the exploitation ability, HMFOA refers to fractional-order calculus, integral and differential operators. In (5), the fractional-order integral operator accumulates $(x_{pi}^j - x_i^j)$ generated by each iteration and calculates the fractional-order integral, further expanding the search scope and improving the global exploration ability. In (6), the fractional-order differential operator subtracts between $(x_{pi}^t - x_i^t)$ and $(x_{pi}^{t-1} - x_i^{t-1})$, calculates the fractional-order differential, which further reduces search range for local exploitation.

$$r_1 = a - \frac{at}{T} \qquad t \in (0, T) \tag{7}$$

$$r_2 = -\frac{a}{T^2}t^2 + a \qquad t \in (0, T) \tag{8}$$
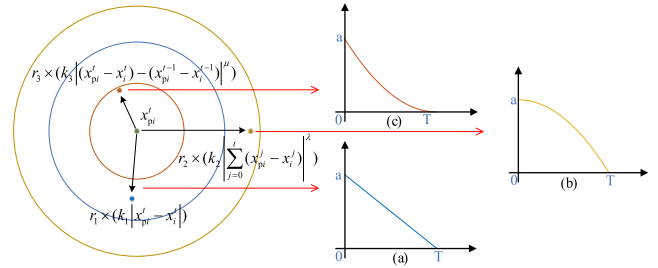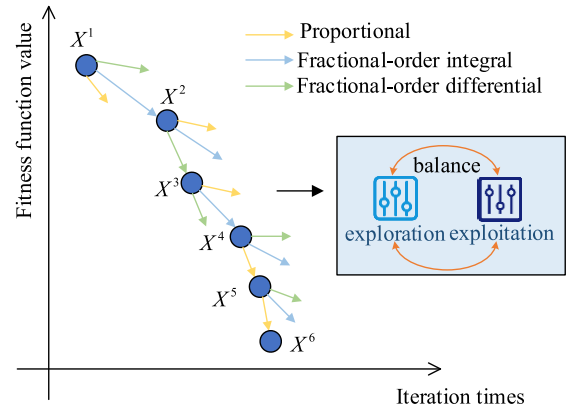
$$r_3 = \frac{a}{T^2}t^2 - \frac{2a}{T}t + a \qquad t \in (0, T) \tag{9}$$

where a is constant; t and T represent iteration and maximum iterations, respectively.

To ensure a smooth transition of the three functions, the initial and ending values of $r_1/r_2/r_3$ are equal, with an initial value of a and an ending value of 0; $r_1/r_2/r_3$ are the corresponding adaptive functions for the proportional operator, fractional-order integral operator, and fractional-order differential operator, respectively, which are shown schematically in (a), (b), and (c) in FIGURE 3. $k_1/k_2/k_3$ is to bring weights before moving the step-size distance, which is applied to determine the direction and range of the iteration position randomly within $[-1,1]$. The value of fractional-order integral order φ sets to $[1,1.5]$; fractional-order differential order δ sets to $[0.5,1]$.

When performing the update directions, each individual has three update strategies with three directions of optimization. In FIGURE 4, a population with an individual is iterated six times for illustration. The initial position is X^1; the three directions of search are proportional, fractional-order integral, and differential directions. The three update directions represent three dimensions for optimization, with different search ranges and different exploration and exploitation abilities (FIGURE 4).

FIGURE 5 gives HMFOA diagram. AlGORITHM 1 shows the steps of the HMFOA.
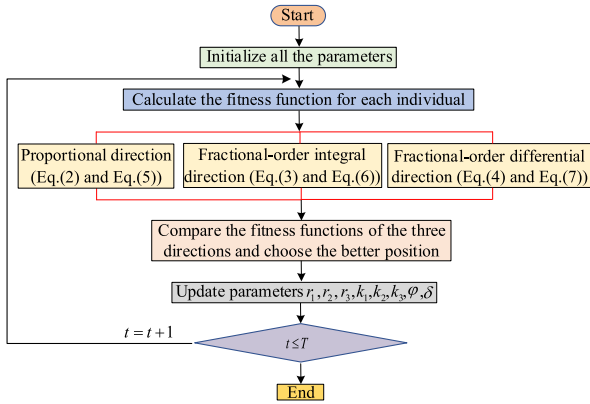
FIGURE 5. Block diagram of HMFOA.

Algorithm 1 Steps of HMFOA

1: Initialize all the parameters ($a = 2$; $T = 200$;

$$r_1 = 2 - \frac{2t}{200} \quad t \in (0, T);$$
$$r_2 = -\frac{2}{200^2}t^2 + 2 \quad t \in (0, T);$$
$$r_3 = \frac{2}{200^2}t^2 - \frac{4}{200}t + 2 \quad t \in (0, T); k_1, k_2, k_3 \in [-1, 1];$$
$$\varphi \in [1, 1.5]; \delta \in [0.5, 1]$$

2: Generate the position of individuals in the initial population
3: while $t \le T$ do
4: Individuals are updated in three search directions: proportional direction ((2) and (5)); fractional-order integral direction (((3) and (6)); and fractional-order differential direction (((4) and (7))
5: Select the position of three smallest fitness in the three search directions for the next iteration
6: Update parameters $r_1, r_2, r_3, k_1, k_2, k_3, \varphi, \delta$
7: End the iteration process
8: Return the optimal solutions

The broad steps of the heuristic optimization algorithm are all consistent. The heuristic optimization algorithms are called by different names because of the different ways of changing the independent variables from the previous generation to the next generation. The computational process from the previous generation to the next generation, the HMFOA proposed in this study only utilizes (4) to (9). (4) to (9) are simple calculations of addition, subtraction, multiplication and division. Therefore, the computational process of the HMFOA proposed in this study is not complicated. Besides, (1) to (3) are employed to introduce the principle of the HMFOA. Consequently, although the HMFOA has a longer name, the HMFOA is still a new type of optimization algorithm formed by the simple operations of addition, subtraction, multiplication, and division within the common optimization algorithms. In addition, the HMFOA
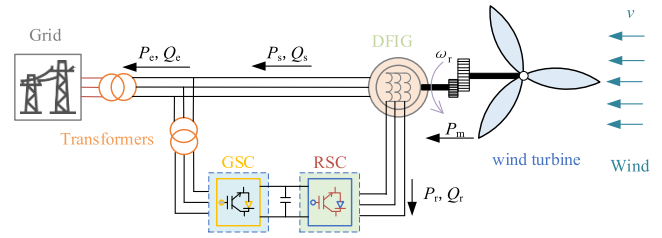
FIGURE 6. Configuration of DFIG-WESs.
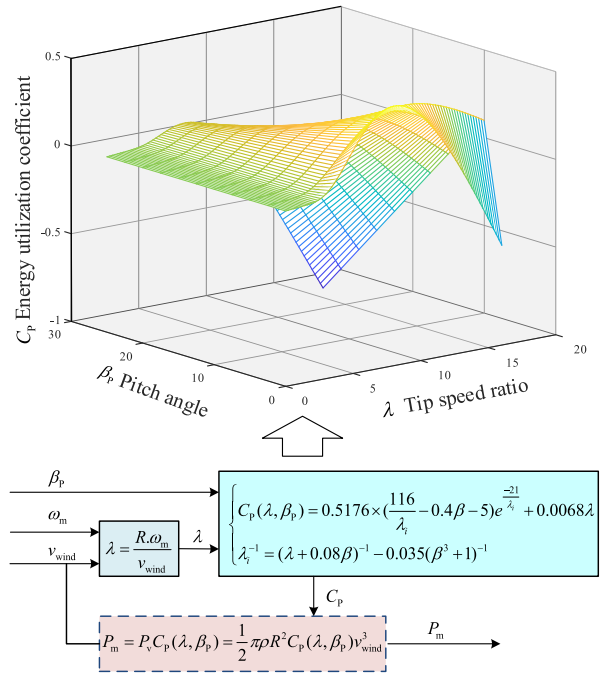
FIGURE 7. Performance curves of variable pitch wind turbines.

formed by addition, subtraction, multiplication, and division operations from (4) to (9) can be easily implemented in practical engineering.

III. MATHEMATICAL MODEL OF DFIG-WESS
The DFIG-WES mainly consists of a wind turbine, a shaft system, a DFIG, a GSC, and an RSC (FIGURE 6). The MPPT seeks to regulate the electromagnetic torque with optimal speed control. The RSC mainly controls the excitation current and torque current. Therefore, the control strategies of MPPT are considered in RSC. GSC is mainly developed to stabilize DC bus voltage and not directly participate in DFIG control.

A. MATHEMATICAL MODEL OF WIND TURBINES
The wind energy utilization coefficient $C_P(\lambda, \beta_P)$, which is a nonlinear function, is a function of λ and β_P. The $C_P - \lambda$ curves of wind turbines depend on the pitch angle β_P (FIGURE 7). In MPPT, to maximize wind energy utilization, the pitch angle β_P should set to be 0. The performance curves of variable pitch wind turbines are displayed in FIGURE 7.

The wind turbine model is [37]:

$$P_{\mathrm{m}} = P_{\mathrm{v}}C_{\mathrm{P}}(\lambda, \beta_{\mathrm{P}}) = \frac{1}{2}\pi\rho R^2 C_{\mathrm{P}}(\lambda, \beta_{\mathrm{P}})v_{\mathrm{wind}}^3 \quad (10)$$

$$C_{\mathrm{P}}(\lambda, \beta_P) = 0.5176 \times (\frac{116}{\lambda_i} - 0.4\beta - 5)e^{\frac{-21}{\lambda_i}}$$
$$+ 0.0068\lambda \quad (11)$$

$$\lambda_i^{-1} = (\lambda + 0.08\beta)^{-1} - 0.035(\beta^3 + 1)^{-1} \quad (12)$$

$$\lambda = \frac{R.\omega_{\mathrm{m}}}{v_{\mathrm{wind}}} \quad (13)$$

where P_{m} means mechanical power output by wind turbine; C_{P} represents power coefficient; λ is tip speed ratio; β_P is pitch angle; P_{v} means the input power of the blade; ρ, R and v_{wind} are air density, wind turbine radius, and wind speed, respectively.

B. MATHEMATICAL MODEL OF DFIGS
The mathematical DFIG is model [38]:

$$\frac{di_{\mathrm{qs}}}{dt} = \frac{\omega_{\mathrm{b}}}{L_{\mathrm{s}}'}(-R_1 i_{\mathrm{qs}} + \omega_{\mathrm{s}}L_{\mathrm{s}}' i_{\mathrm{qs}} + \frac{\omega_{\mathrm{r}}}{\omega_{\mathrm{s}}}e_{\mathrm{qs}}' - \frac{1}{T_{\mathrm{r}}\omega_{\mathrm{s}}}e_{\mathrm{ds}}'$$
$$- v_{\mathrm{qs}} + \frac{L_{\mathrm{m}}}{L_{\mathrm{rr}}}v_{\mathrm{qr}}) \quad (14)$$

$$\frac{di_{\mathrm{ds}}}{dt} = \frac{\omega_{\mathrm{b}}}{L_{\mathrm{s}}'}(-w_{\mathrm{s}}L_{\mathrm{s}}' i_{\mathrm{qs}} - R_1 i_{\mathrm{qs}} + \frac{1}{T_{\mathrm{r}}\omega_{\mathrm{s}}}e_{\mathrm{qs}}' + \frac{\omega_{\mathrm{r}}}{\omega_{\mathrm{s}}}e_{\mathrm{ds}}'$$
$$- v_{\mathrm{ds}} + \frac{L_{\mathrm{m}}}{L_{\mathrm{rr}}}v_{\mathrm{qr}}) \quad (15)$$

$$\frac{de_{\mathrm{qs}}'}{dt} = \omega_{\mathrm{b}}\omega_{\mathrm{s}}[R_2 i_{\mathrm{ds}} - \frac{1}{T_{\mathrm{r}}\omega_{\mathrm{s}}}e_{\mathrm{qs}}' + (1 - \frac{\omega_{\mathrm{r}}}{\omega_{\mathrm{s}}})e_{\mathrm{ds}}' - \frac{L_{\mathrm{m}}}{L_{\mathrm{rr}}}v_{\mathrm{qr}}]$$
$$(16)$$

$$\frac{de_{\mathrm{ds}}'}{dt} = \omega_{\mathrm{b}}\omega_{\mathrm{s}}[-R_2 i_{\mathrm{qs}} - (1 - \frac{\omega_{\mathrm{r}}}{\omega_{\mathrm{s}}})e_{\mathrm{qs}}' - \frac{1}{T_{\mathrm{r}}\omega_{\mathrm{s}}}e_{\mathrm{ds}}' + \frac{L_{\mathrm{m}}}{L_{\mathrm{rr}}}v_{\mathrm{qr}}]$$
$$(17)$$

$$T_{\mathrm{e}} = (e_{\mathrm{qs}}'/\omega_{\mathrm{s}})i_{\mathrm{qs}} + (e_{\mathrm{ds}}'/\omega_{\mathrm{s}})i_{\mathrm{ds}} \quad (18)$$

$$P_{\mathrm{e}} = e_{\mathrm{qs}}' i_{\mathrm{qs}} + e_{\mathrm{ds}}' i_{\mathrm{ds}} \quad (19)$$

$$Q_{\mathrm{s}} = v_{\mathrm{qs}} i_{\mathrm{ds}} \quad (20)$$

where ω_{b} and ω_{s} are electrical base speed and rotational speed of the synchronous, respectively; ω_{r} represents rotor angular speed; e_{ds}' and e_{qs}' represent dq-axis equivalent internal voltages; i_{ds} and i_{qs}, v_{ds} and v_{qs}, v_{dr} and v_{qr} imply dq-stator currents, stator external voltages and rotor voltages; L_{m} and L_{s}' are mutual and stator inductances, respectively; R_1, R_2, T_{r} and L_{rr} are intermediate variables;$T_{\mathrm{r}} = L_{\mathrm{rr}}/R_{\mathrm{r}}$;$L_{\mathrm{rr}} = 1.005 \times 1.01L_{\mathrm{m}}$; $L_{\mathrm{s}}' = 1.01L_{\mathrm{m}}$; R_s indicates the stator resistance; R_r is the rotor resistance; the electromagnetic torque generated by the DFIG is T_{e}; v_{qs} means terminal voltage amplitude.

C. MATHEMATICAL MODELING OF SHAFT SYSTEMS
A single centralized inertial system can represent the rotating shaft system [39].

$$H_{\mathrm{m}} = H_{\mathrm{t}} + H_g \quad (21)$$

$$\frac{d\omega_{\mathrm{m}}}{dt} = \frac{1}{2H_{\mathrm{m}}}(T_{\mathrm{m}} - T_{\mathrm{e}} - D_{\mathrm{LS}}\omega_{\mathrm{m}}) \quad (22)$$

FIGURE 8. DFIG-WES framework.

where H_{m} means concentrated inertia constant; the electromagnetic dynamic equation in the shaft system is shown in (21); ω_{m} means rotational speed; $\omega_{\mathrm{r}} = \omega_{\mathrm{m}}$; D_{LS} means lumped system damping; T_{m} means mechanical torque;

D. CONTROL STRUCTURE OF ROTOR SIDE CONTROLLERS
There are two main control objectives of the DFIG: (i) to achieve MPPT under the condition of variable speed constant frequency by controlling the rotor speed or active power; (ii) to assure the stability of the power grid by controlling the reactive output power. The RSC aims to realize the effective control of the two-component currents of the rotor. In this study, the VC framework of four HDMFOCs is applied to control the DFIG (FIGURE 8). The external control loop obtains the dq-axis rotor current base values i_{qr}^* and i_{dr}^* by adjusting rotor speed and reactive power, respectively; the internal control loop controls the two currents related to the compensation terms v_{dr2} and v_{qr2} for generating the final outputs v_{dr} and v_{qr} of the controllers. The associated variables are as follows [40].

$$v_{\mathrm{dr}} = R_{\mathrm{r}}i_{\mathrm{dr}} + \sigma L_{\mathrm{r}}\frac{di_{\mathrm{dr}}}{dt} - s\omega_{\mathrm{s}}\sigma L_{\mathrm{r}}i_{\mathrm{qr}} \quad (23)$$

$$v_{\mathrm{qr}} = R_{\mathrm{r}}i_{\mathrm{qr}} + \sigma L_{\mathrm{r}}\frac{di_{\mathrm{qr}}}{dt} - s\omega_{\mathrm{s}}\left(\frac{L_{\mathrm{m}}^2}{L_{\mathrm{s}}}i_{\mathrm{ms}} + \sigma L_{\mathrm{r}}i_{\mathrm{dr}}\right) \quad (24)$$

$$\psi_{\mathrm{s}} = L_{\mathrm{m}}I_{\mathrm{ms}} \quad (25)$$

$$s = \frac{\omega_{\mathrm{s}} - \omega_{\mathrm{r}}}{\omega_{\mathrm{s}}} \quad (26)$$

$$\sigma = 1 - \frac{L_{\mathrm{m}}^2}{L_{\mathrm{s}}L_{\mathrm{r}}} \quad (27)$$

$$i_{\mathrm{ms}} = \frac{v_{\mathrm{qs}} - R_s i_{\mathrm{qs}}}{\omega_{\mathrm{s}}L_{\mathrm{m}}} \quad (28)$$

where s is slip ratio; σ is leakage coefficient.

In the RSC of DFIG, the vector control loop is composed of four HDMFOCs. The control objects are ω_{r}, Q_s, i_{dr}, and i_{qr}, respectively. As shown in FIGURE 8, two fractional orders calculate the information of each dimension. Therefore, there are eight parameters to be optimized for each HDMFOC.

TABLE 2. Eight benchmark function formulas and objective function values.

F	Function	n	Range	f_j^{min}
F1	$f_1(x) = \sum_{i=1}^{n} x_i^2$	30	[-100,100]	0
F2	$f_2(x) = \sum_{i=1}^{n}|x_i| + \prod_{i=1}^{n}|x_i|$	30	[-10,10]	0
F3	$f_3(x) = \sum_{i=1}^{n}(\sum_{j-1}^{i} x_j)^2$	30	[-100,100]	0
F4	$f_4(x) = \max_i\{|x_i|, 1 \le i \le n\}$	30	[-100,100]	0
F5	$f_5(x) = \sum_{i=1}^{n} ix_i^4 + random[0,1)$	30	[-1.28,1.28]	0
F6	$f_6(x) = \sum_{i=1}^{n} x_i^2 - 10\cos(2\pi x_i) + 10$	30	[-5.12,5.12]	0
F7	$f_7(x) = -20\exp(-0.2\sqrt{\frac{1}{n}\sum_{i=1}^{n} x_i^2}) - \exp(\frac{1}{n}\sum_{i=1}^{n}\cos(2\pi x_i)) + 20 + e$	30	[-32,32]	0
F8	$f_8(x) = \frac{1}{4000}\sum_{i=1}^{n} x_i^2 - \prod_{i=1}^{n}\cos(\frac{x_i}{\sqrt{i}}) + 1$	30	[-600,600]	0

IV. CASE STUDIES

The case studies are run at MATLAB/Simulink 9.2 in a computer with 3.60 GHz CPU and 16 GB RAM.

The proposed HMFOA is compared under two cases, including the benchmark functions (Case I) and the parameter tuning of the DFIG (Case II). The performance of HMFOA is tested with unimodal benchmark functions and multimodal benchmark functions in Case I. The HMFOA is compared with other 18 intelligent optimization algorithms In Case II, the proposed HMFOA is applied to the MPPT of the DFIG to tune the control parameters of four HDMFOCs of the RSC and is compared with the other four intelligent optimization algorithms of the MFO, ant lion optimization (ALO), dragonfly algorithm (DA), and SCA.

A. CASE I

In Case I, the HMFOA is compared with the other 18 intelligent optimization algorithms. The eight benchmark function formulas and objective function values are given in TABLE 2. The benchmark functions F1 through F8 are all functions in CEC. Since F5, F6, and F7 contain random numbers, F5, F6, and F7 describe extremely complex scenarios. The 19 intelligent optimization algorithms are all calculated under the same conditions: i) the population size, or the number of individuals N_{size} of all algorithms is 100; ii) the maximum number of iterations T of all algorithms is 500; iii) fitness function values of all algorithms are averaged after ten runs. The unimodal (FIGURE 9(a)-9(e)) and multimodal benchmark functions (FIGURE 9(g)-9(h)) are applied to test 19 intelligent optimization algorithms.

The numerical results of fitness function values tested by 19 intelligent optimization algorithms (TABLE 3) show that the HMFOA obtains the smallest fitness values than the other 18 intelligent optimization algorithms. The HMFOA has a higher optimization ability. The box-and-whisker plots (FIGURE 10) compare the fitness functions for the 19 intelligent optimization algorithms after ten runs. Box and whisker plot is a statistical chart showing the dispersion of a group
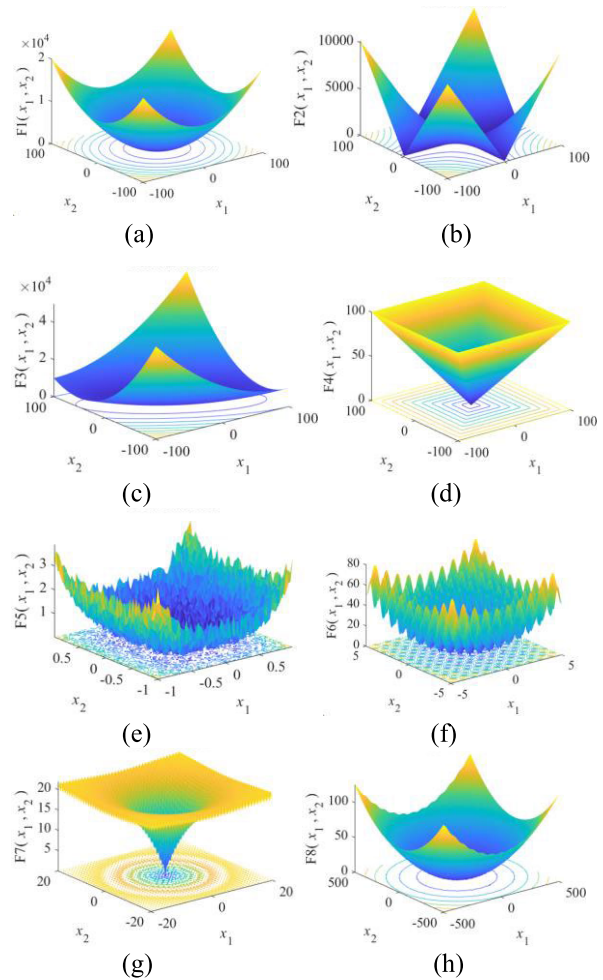
FIGURE 9. Function diagrams of eight benchmark functions (F1 to F8).

TABLE 3. Fitness values obtained by 19 intelligent optimization algorithms.

Algorithm	Fit1	Fit2	Fit3	Fit4	Fit5	Fit6	Fit7	Fit8
1.MVO	0.7699	0.5949	91.0510	1.2336	0.0179	135.6116	0.3793	0.7707
2.GA	0.0253	1.1666	3.7144	1.8387	0.4461	8.0433	0.2278	0.0044
3.PSO	0.1886	1.8051	618.7608	11.8849	0.1479	64.5249	0.9220	0.1986
4.BBO	1.5813	0.4065	325.2028	1.1531	0.0072	37.0100	0.0234	0.9319
5.MFO	2.3164	30.0924	2.57×10^6	62.9319	1.7342	150.4943	0.2119	18.9376
6.ALO	1.1×10^4	35.0566	1980.5025	12.7968	0.1163	68.1546	0.9203	0.0142
7.DA	716.2230	13.6630	6788.6878	19.6129	0.3183	143.5486	3.2520	8.1815
8.GSO	0.0071	0.0486	1119.9638	4.9739	0.0663	15.6635	7.70×10^4	0.0355
9.SCA	1.6698	0.0223	5236.3468	35.2612	0.0335	35.4143	4.3737	0.7449
10.ACOR	3324.7072	9.68×10^7	1.08×10^6	84.1192	13.3760	305.1385	0.0028	26.1874
11.FA	9.23×10^8	1.30×10^4	1.01×10^6	1.4×10^4	0.0014	62.1847	3.74×10^5	0.1810
12.ICA	3.90×10^6	5.56×10^5	2569.1114	13.7796	0.1284	54.3717	2.24×10^8	0.0525
13.CA	17.7061	4.7698	7668.4917	43.3770	0.3730	114.4900	1.2142	0.6083
14.ABC	8.0310	20.0850	6.71×10^5	56.7940	0.4005	237.6229	0.0070	1.0765
15.IWO	1.99×10^7	0.0578	2.86×10^5	53.9807	0.0335	67.1787	18.2408	529.1616
16.SPEA2	1986.3160	16.3901	6968.2237	25.8956	0.2989	105.1042	5.8350	20.8709
17.DE	5.2×10^4	0.0024	3.05×10^5	12.8645	0.0511	85.9970	1.23×10^6	0.0086
18.HS	513.7544	4.0364	3.81×10^5	26.4862	0.2641	22.9566	0.2633	5.4589
19.HMFOA	2.73×10^{20}	3.84×10^{14}	8.65×10^7	5.22×10^6	4.1×10^4	0.9950	7.97×10^{11}	1.91×10^3

of data. FIGURE 10 shows that the box-and-whisker plot of the HMFOA is more aggregated, which shows that the results of each optimization are similar. HMFOA has the stability of operations.

FIGURE 11 gives search history of 500 iterations and the last 100 iterations. In FIGURE 11, in the early process of search history, the search agents approach the target position at a faster rate; in the latter process of search history, the search agents approach the target position at a relatively small rate to converge to the target position accurately. The
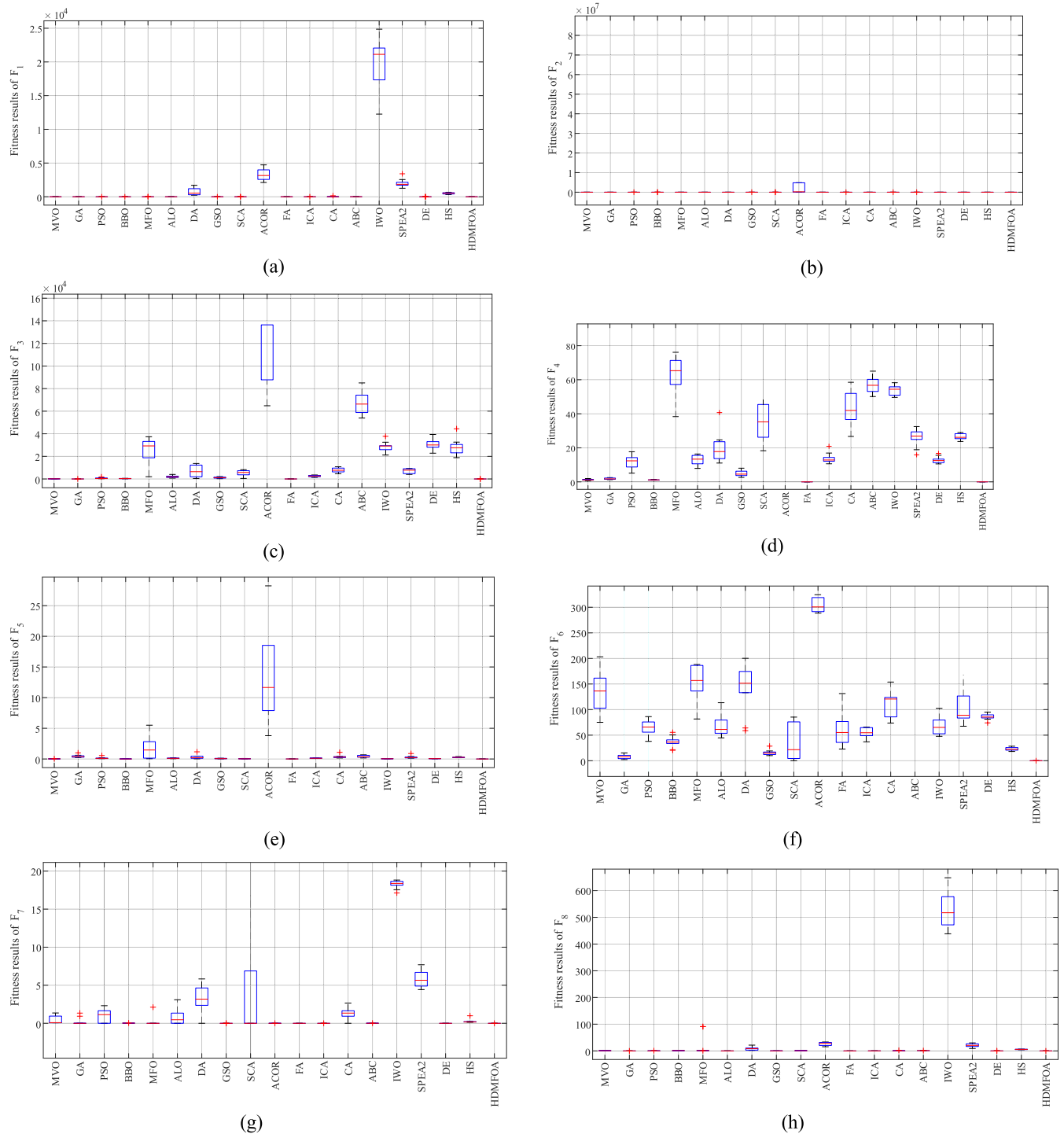
FIGURE 10. Box-and-whisker plots of fitness function of eight benchmark functions (F1 to F8).

HMFOA has strong exploration ability in the early process of optimization and strong exploitation ability in the latter optimization process. The HMFOA realizes multi-directional optimization in the optimization process, decides exploration or exploitation according to the previous iteration process, and achieves the balance of exploration and exploitation.

FIGURE 12 shows the convergence curves of the HMFOA, which includes the ordinary convergence curve and the convergence curve taking the logarithm of the fitness function value, which can clearly show the change of fitness function value in the latter search process. The HMFOA has great convergence on the benchmark function test and transitions from
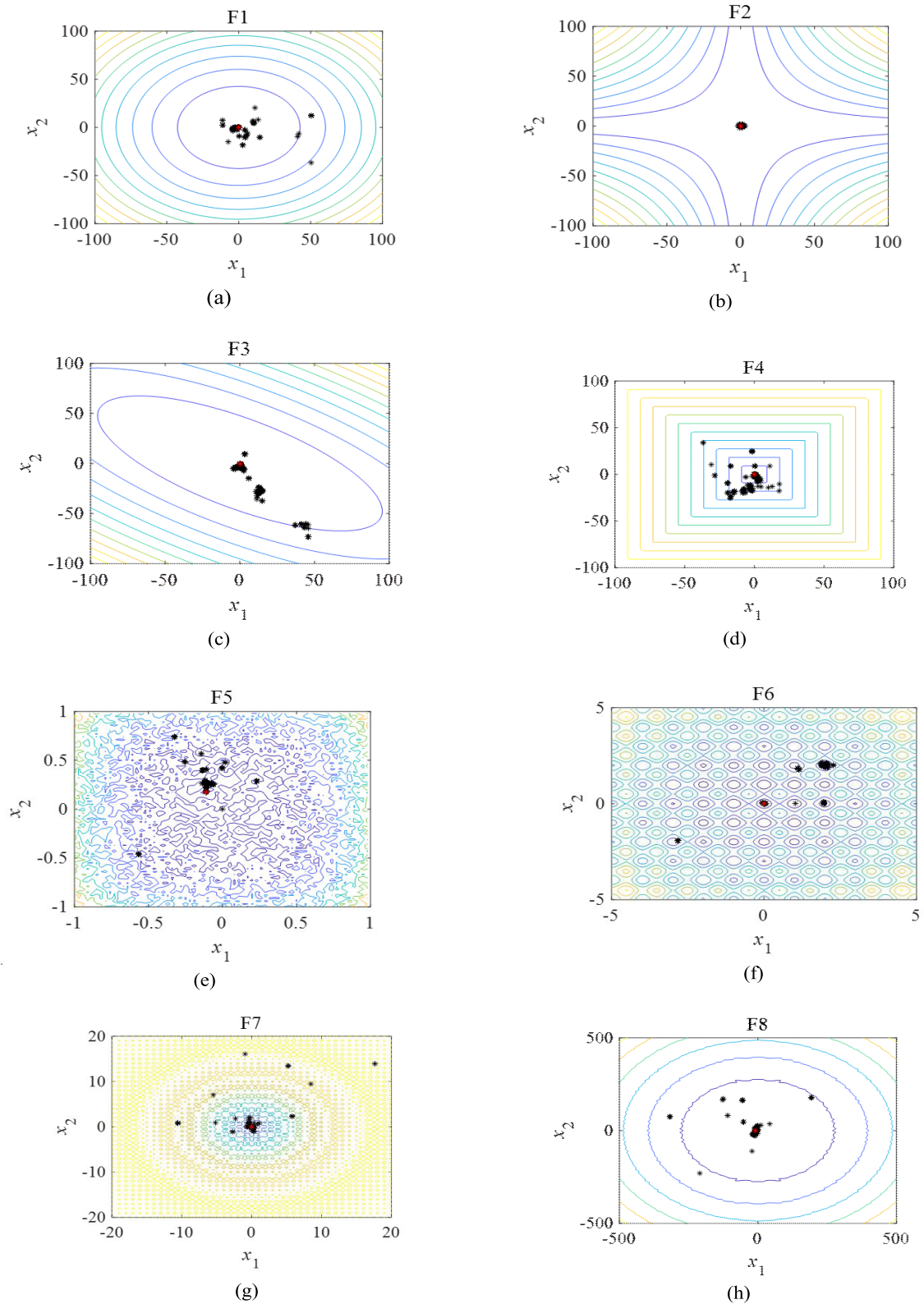
FIGURE 11. Search history of search agents in eight benchmark functions (F1 to F8).

the overall exploration process to the exploitation process at about 100 iterations, with strong exploration capability in

the earlier search process. The convergence curve of taking logarithm can be seen in the HMFOA in the later search
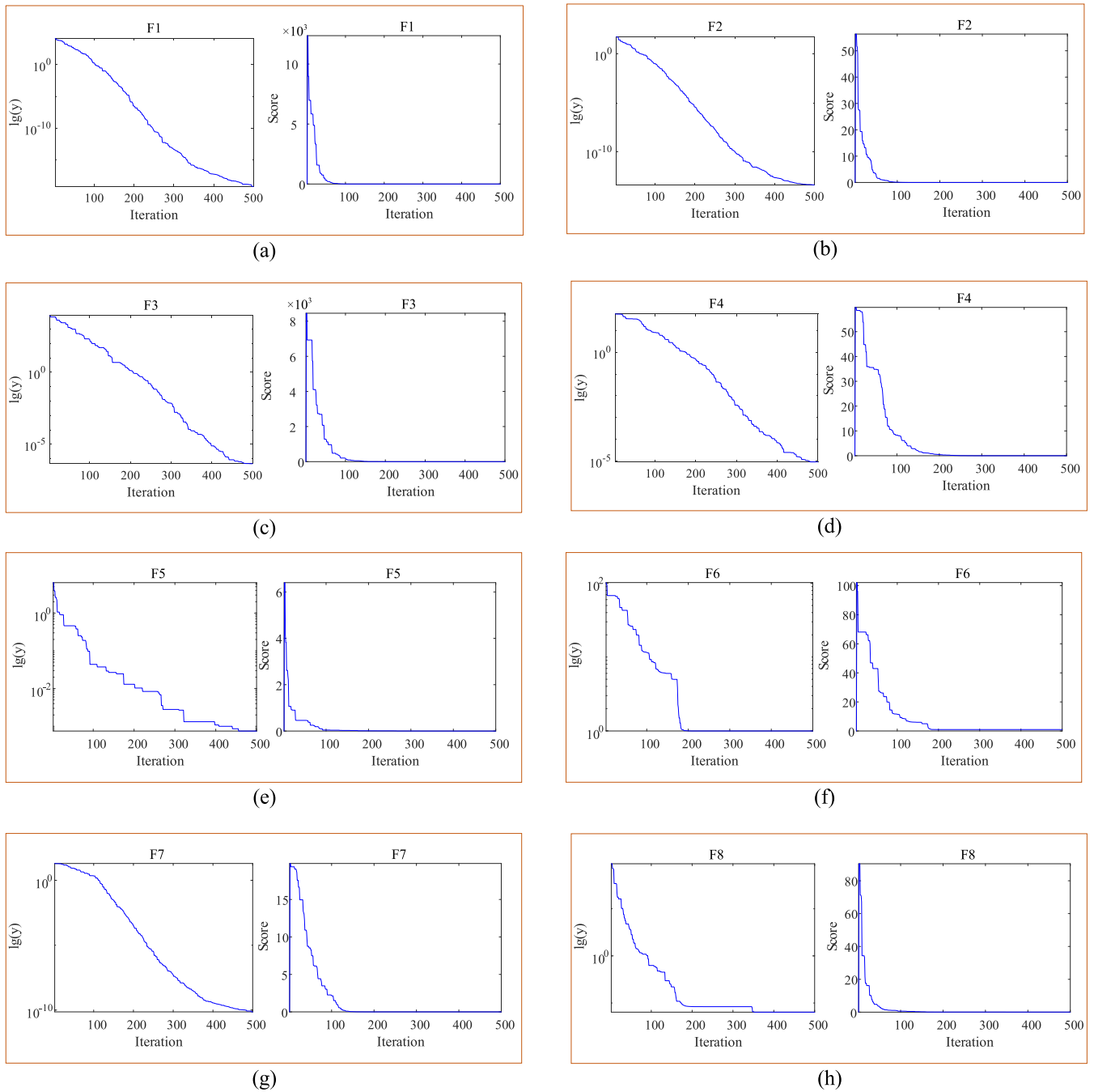
FIGURE 12. Convergence curve of high-dimensional multiple fractional-order optimization algorithm (F1 to F8).

process in a smaller rate change, which demonstrates the HMFOA has a strong ability to exploit with high accuracy.

FIGURE 13 shows the average fitness values during the optimization of the benchmark function. In the optimization process, the average fitness function value gradually decreases and tends to converge. The high fluctuation of fitness function indicates that the deterioration of fitness function is inevitable in the earlier process of continuous exploration.

B. CASE II

The HMFOA is applied to the MPPT of the DFIG. The RSC contains four HDMFOCs. Each HDMFOC contains eight parameters that need to be optimized. The control objective in this study is to minimize the error of reactive power and rotor speed under various conditions. The objective function and constraints are shown below:

$$f_{\text{total}}(x) = f_1(x) + f_2(x) + f_3(x) \tag{29}$$
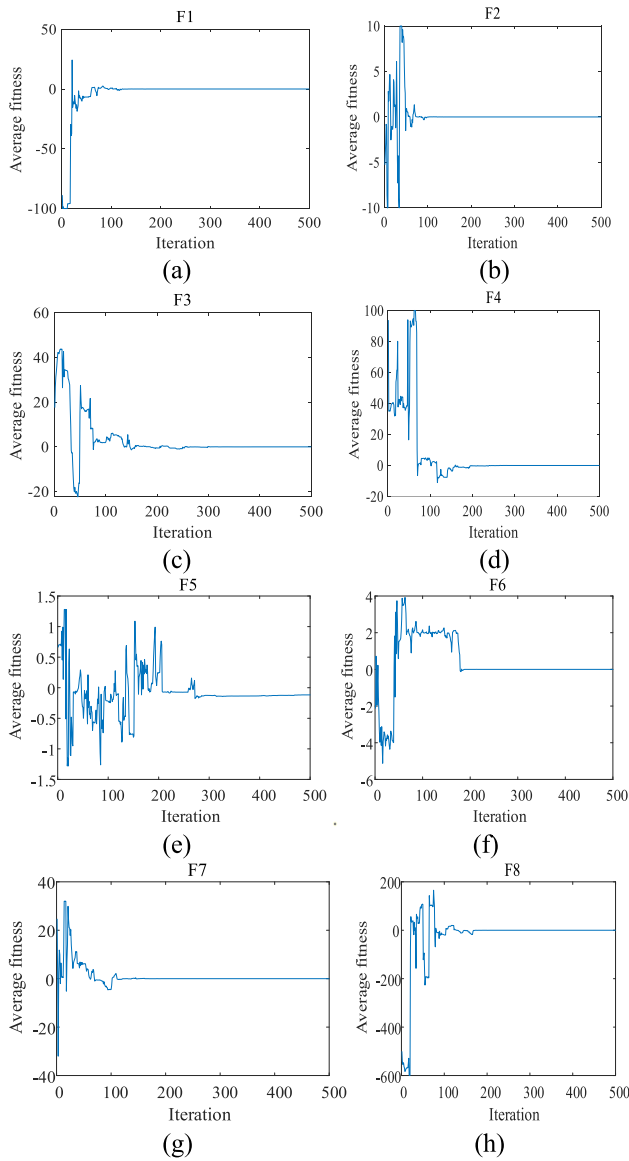
FIGURE 13. Average fitness value in optimization process (F1 to F8).

$$f_i(x) = \int_0^{T_{DFIG}} (\varphi_1 |Q_s - Q_s^*| + \varphi_2 |\omega_r - \omega_r^*|)\mathrm{d}t \quad (30)$$

$$s.t. \begin{cases} v_{wind}^{min} < v_{wind} < v_{wind}^{max} \\ V_s^{min} < V_s < V_s^{max} \\ Q_s^{min} < Q_s < Q_s^{max} \end{cases} \quad (31)$$

where $f_1(x)$, $f_2(x)$ and $f_3(x)$ represent the objective function (FIGURE 14); where Q_s, v_{wind}, V_s and ω_r represent reactive power, wind speed, power grid voltage, and rotor angular speed, respectively. Step wind speed reflects the sudden variability between 8-12 m/s; where T_{DFIG} is the running time of the DFIG in Case II; the wind speed range v_{wind} is [8, 12] m/s. The system parameters of DFIG-WES are presented in TABLE 4. φ_1 and φ_2 are the coefficients of reactive power and rotor speed errors in the objective function, respectively. The unit values of reactive power and rotor speed
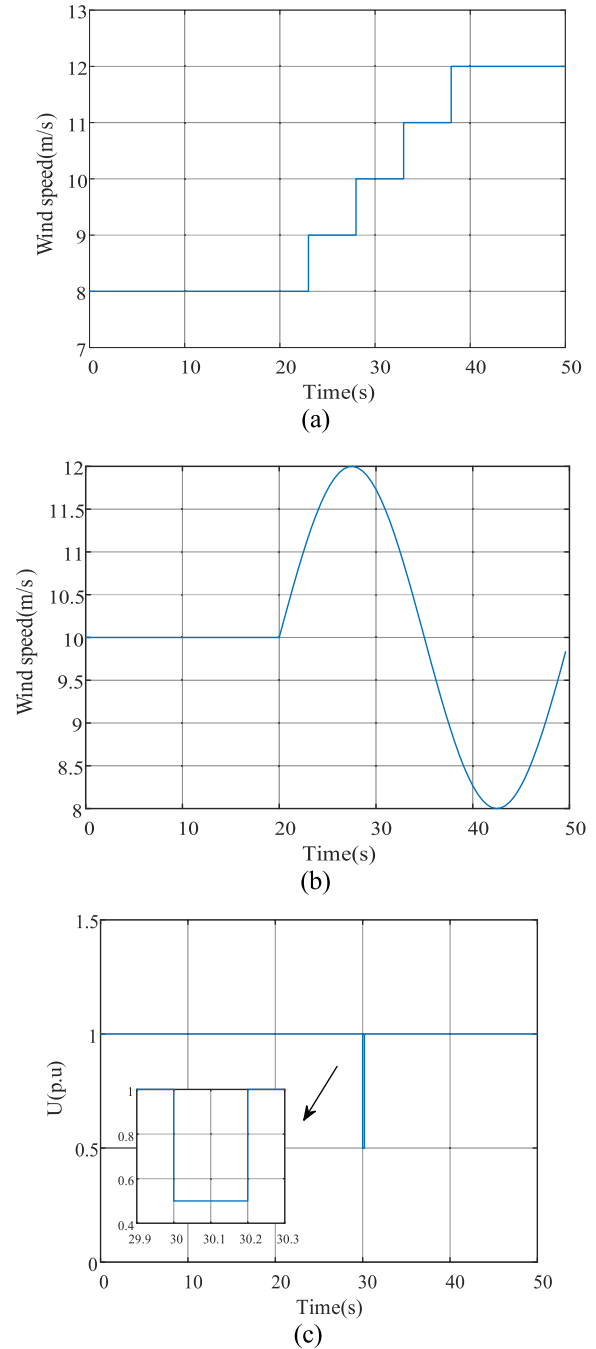
FIGURE 14. Schematic diagrams of three operating conditions under Case II: (a) step wind speed; (b) gradual wind speed; (c) voltage drop.

errors are different; different coefficients should balance the importance of the two objectives. After continuous manual debugging, it is relatively appropriate to set φ_1 to 0.04 and set φ_2 to 1.

The five heuristic optimization algorithms (i.e., MFO, ALO, DA, SCA, and HMFOA) are all calculated under the same conditions: i) the population size and individual number N_{size} of all algorithms is 100; (ii) the fitness function values of all algorithms are compared after ten runs. It is noted that the selection of the maximum iterations T determines the
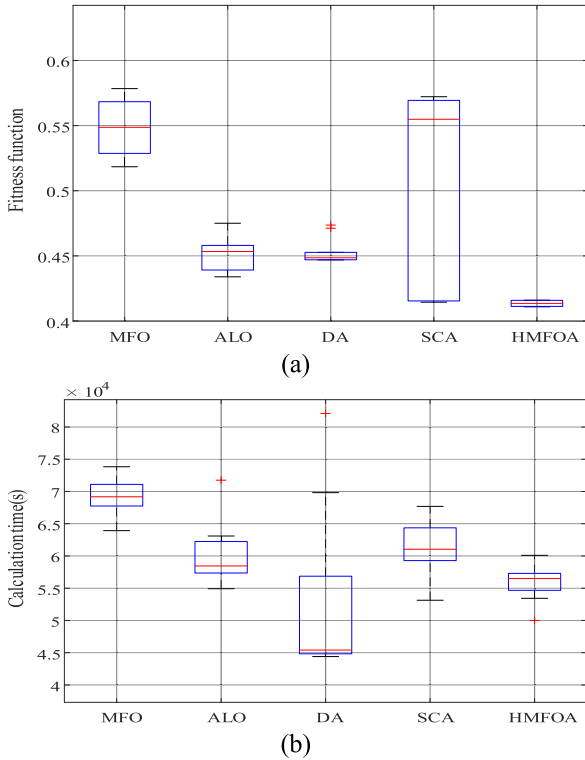
FIGURE 15. Box-and-whisker plots of five intelligent optimization algorithms: (a) fitness function; (b) calculation time.

TABLE 4. Control parameters of moth-flame optimization algorithm.

Symbols	K_{Q1}	K_{Q2}	K_{Q3}	K_{Q4}	α_{Q1}	α_{Q2}	α_{Q3}	α_{Q4}
Value	-0.17553	0.79630	0.17422	0.03562	-0.00013	0.00870	0.00229	0.00023
Symbols	K_{Id1}	K_{Id2}	K_{Id3}	K_{Id4}	α_{Id1}	α_{Id2}	α_{Id3}	α_{Id4}
Value	0.12449	-0.00114	0.00642	-0.00112	0.18538	-0.00048	-0.00021	-6.76×10^{-5}
Symbols	$K_{\omega r1}$	$K_{\omega r2}$	$K_{\omega r3}$	$K_{\omega r4}$	$\alpha_{\omega r1}$	$\alpha_{\omega r2}$	$\alpha_{\omega r3}$	$\alpha_{\omega r4}$
Value	42.90898	159.51871	19.08527	26.66678	-0.00096	0.01827	0.00083	-0.00155
Symbols	K_{Iq1}	K_{Iq2}	K_{Iq3}	K_{Iq4}	α_{Iq1}	α_{Iq2}	α_{Iq3}	α_{Iq4}
Value	0.03042	0.00075	-1.83×10^{-5}	-2.41×10^{-5}	0.47987	-0.00078	-1.59×10^{-5}	0.00153

TABLE 5. Control parameters of ant lion optimization algorithm.

Symbols	K_{Q1}	K_{Q2}	K_{Q3}	K_{Q4}	α_{Q1}	α_{Q2}	α_{Q3}	α_{Q4}
Value	-0.22513	0.58036	0.08991	0.05030	-0.00022	0.00596	0.00110	0.00050
Symbols	K_{Id1}	K_{Id2}	K_{Id3}	K_{Id4}	α_{Id1}	α_{Id2}	α_{Id3}	α_{Id4}
Value	0.10915	-0.00096	0.01254	-0.00499	0.11495	-0.00461	-0.00058	-0.00013
Symbols	$K_{\omega r1}$	$K_{\omega r2}$	$K_{\omega r3}$	$K_{\omega r4}$	$\alpha_{\omega r1}$	$\alpha_{\omega r2}$	$\alpha_{\omega r3}$	$\alpha_{\omega r4}$
Value	26.30313	70.83533	5.04300	39.05875	-0.00078	0.02525	0.00423	-0.00175
Symbols	K_{Iq1}	K_{Iq2}	K_{Iq3}	K_{Iq4}	α_{Iq1}	α_{Iq2}	α_{Iq3}	α_{Iq4}
Value	0.09826	0.00447	-9.70×10^{-5}	-3.82×10^{-5}	0.21070	-0.00158	-2.06×10^{-5}	0.00337

quality of the optimal solution and operation time. Choosing a larger T means a higher quality optimal solution but leads to a longer operation time. In this paper, trial-and-error shows that when $T = 200$, the fitness function value remains unchanged or slightly changes. Therefore, T is set to 200 to obtain a better fitness function value and shorten the operation time of algorithms.

Box-and-whisker plot describes the discrete distribution of data in a relatively stable way. As shown in FIGURE 15(a), the two algorithms of DA and HMFOA have a small range between the upper and lower limits of the fitness function values, with a more concentrated distribution and great convergence stability. Among the five intelligent optimization algorithms, the fitness function obtained by HMFOA is the smallest, which indicates that the control parameters are optimal. As shown in FIGURE 15 (b), the calculation time of HMFOA is small. Although the computation time of HMFOA is larger than that of DA, the value of the fitness function is lower than that of DA. Compared to DA, HMFOA takes more computational time for exploration.

FIGURE 16 shows that: i) the overshoot of rotor speed error obtained by the HMFOA is the smallest; ii) the HMFOA can obtain the accurate maximum power coefficient and wind energy capture of the DFIG. Although the active and reactive power deviations in FIGURE 16 appear large, the overall deviation is small.

The system response curves (FIGURE 17(a) and FIGURE 17(c)) illustrate that the rotor speed deviation and reactive power deviation of HMFOA have the smallest oscillation, which has a smoother control performance compared with the other four algorithms. Besides, the DFIG based on the HMFOA can maintain the optimal power coefficient and better realize the maximum wind energy tracking (FIGURE 17(b) and FIGURE 17(d)).

Power grid fault or load change could lead to a sudden voltage drop, which requires the DFIG to have a certain ability to recover the system and ensure that the DFIG does not go off the grid. The system response diagram of DFIG to the voltage drop (FIGURE 18) shows that the HMFOA can recover to the stable state of the system with the fastest speed and minimum fluctuation. Therefore, the HMFOA has a certain system recovery ability.

Since the MPPT of the DFIG is not a theoretically analyzable problem, no theoretically optimal solution exists. If the theoretically optimal curve can be found, then the HMFOA proposed in this study is not necessary to exist. In addition, the HMFOC proposed in this study is precisely the solution to the problem of optimal solutions that are not theoretically findable.

The HMFOA and other intelligent optimization algorithms are offline optimizations rather than online optimizations. The control parameters of HDMFOCs can be directly applied in the HDMFOCs after tuning with the optimization algorithms. The calculation time of these compared algorithms is long (at the hourly level), which cannot meet the continuous control of the MPPT (at the millisecond level) and faults in the power grid. TABLE 4 to TABLE 8 are the control parameters of the DFIG obtained by these five compared algorithms.

TABLE 9 compares the operation time, the best, the worst, average objective values, the standard deviation, and the relative standard deviation. Compared with four other algorithms, the average operation time of HMFOA is 14.5750 hours,
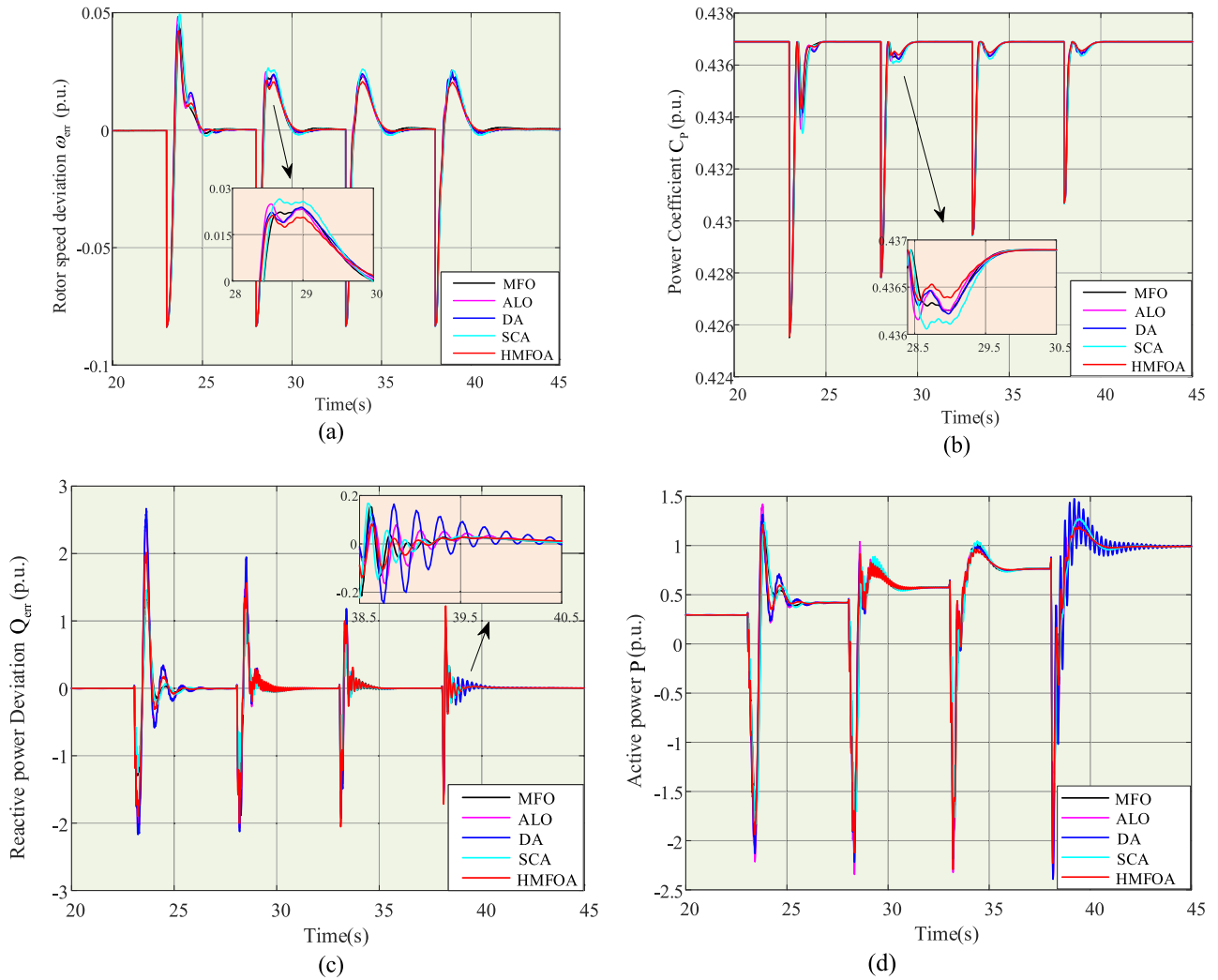
FIGURE 16. System response diagrams under stepped wind speed condition of Case II: (a) curves of rotor speed deviation; (b) curves of power coefficient; (c) curves of reactive power deviation; (d) curves of active power.

TABLE 6. Control parameters of dragonfly algorithm optimization algorithm.

Symbols	K_{Q1}	K_{Q2}	K_{Q3}	K_{Q4}	α_{Q1}	α_{Q2}	α_{Q3}	α_{Q4}
Value	-0.18339	0.48856	0.06361	0.01994	-0.00064	0.00698	0.00190	0.00034
Symbols	K_{Id1}	K_{Id2}	K_{Id3}	K_{Id4}	α_{Id1}	α_{Id2}	α_{Id3}	α_{Id4}
Value	0.11011	-0.00039	0.01467	-0.00650	0.07682	-0.00457	-0.00066	-0.00018
Symbols	$K_{\omega r1}$	$K_{\omega r2}$	$K_{\omega r3}$	$K_{\omega r4}$	$\alpha_{\omega r1}$	$\alpha_{\omega r2}$	$\alpha_{\omega r3}$	$\alpha_{\omega r4}$
Value	15.10177	61.88095	6.14370	31.71634	-0.00069	0.05469	0.00676	-0.00203
Symbols	K_{Iq1}	K_{Iq2}	K_{Iq3}	K_{Iq4}	α_{Iq1}	α_{Iq2}	α_{Iq3}	α_{Iq4}
Value	0.13064	0.00949	-0.00012	-1.26×10⁻⁵	0.15794	-0.00167	-3.32×10⁻⁵	0.00437

TABLE 7. Control parameters of sine cosine optimization algorithm.

Symbols	K_{Q1}	K_{Q2}	K_{Q3}	K_{Q4}	α_{Q1}	α_{Q2}	α_{Q3}	α_{Q4}
Value	-0.27775	0.87541	0.18605	0.00858	-7.39×10⁻⁵	0.00281	0.00053	7.26×10⁻⁵
Symbols	K_{Id1}	K_{Id2}	K_{Id3}	K_{Id4}	α_{Id1}	α_{Id2}	α_{Id3}	α_{Id4}
Value	0.15004	-0.00124	0.00656	-0.00059	0.13943	-0.00044	-0.00020	-1.77×10⁻⁵
Symbols	$K_{\omega r1}$	$K_{\omega r2}$	$K_{\omega r3}$	$K_{\omega r4}$	$\alpha_{\omega r1}$	$\alpha_{\omega r2}$	$\alpha_{\omega r3}$	$\alpha_{\omega r4}$
Value	111.64928	187.11503	16.83044	36.78282	-0.00057	0.02314	0.00087	-0.00089
Symbols	K_{Iq1}	K_{Iq2}	K_{Iq3}	K_{Iq4}	α_{Iq1}	α_{Iq2}	α_{Iq3}	α_{Iq4}
Value	0.01154	0.01278	-2.37×10⁻⁵	-3.32×10⁻⁶	0.71991	-0.00112	-9.87×10⁻⁶	0.00352

which is only more than that of DA. The HMFOA can obtain the minimum objective function value, which is 0.4107. The average objective value of the minimum fitness function is 0.4135, which shows that the HMFOA can effectively tune the optimal control parameters.

C. DISCUSSIONS

The HDMFOC inspires the HMFOA with three dimensions of search directions. Collaborative search with three search directions with different exploration and exploitation abilities can improve the accuracy of the search. The characteristics of the HMFOA can be summarized below.

1) The HMFOA embraces three-dimensional search directions, namely, proportional direction, fractional-order differential direction, and fractional-order differential direction, which can balance exploration and exploitation. The introduction of fractional calculus orders can expand the search area. The fractional-order differential direction has a strong
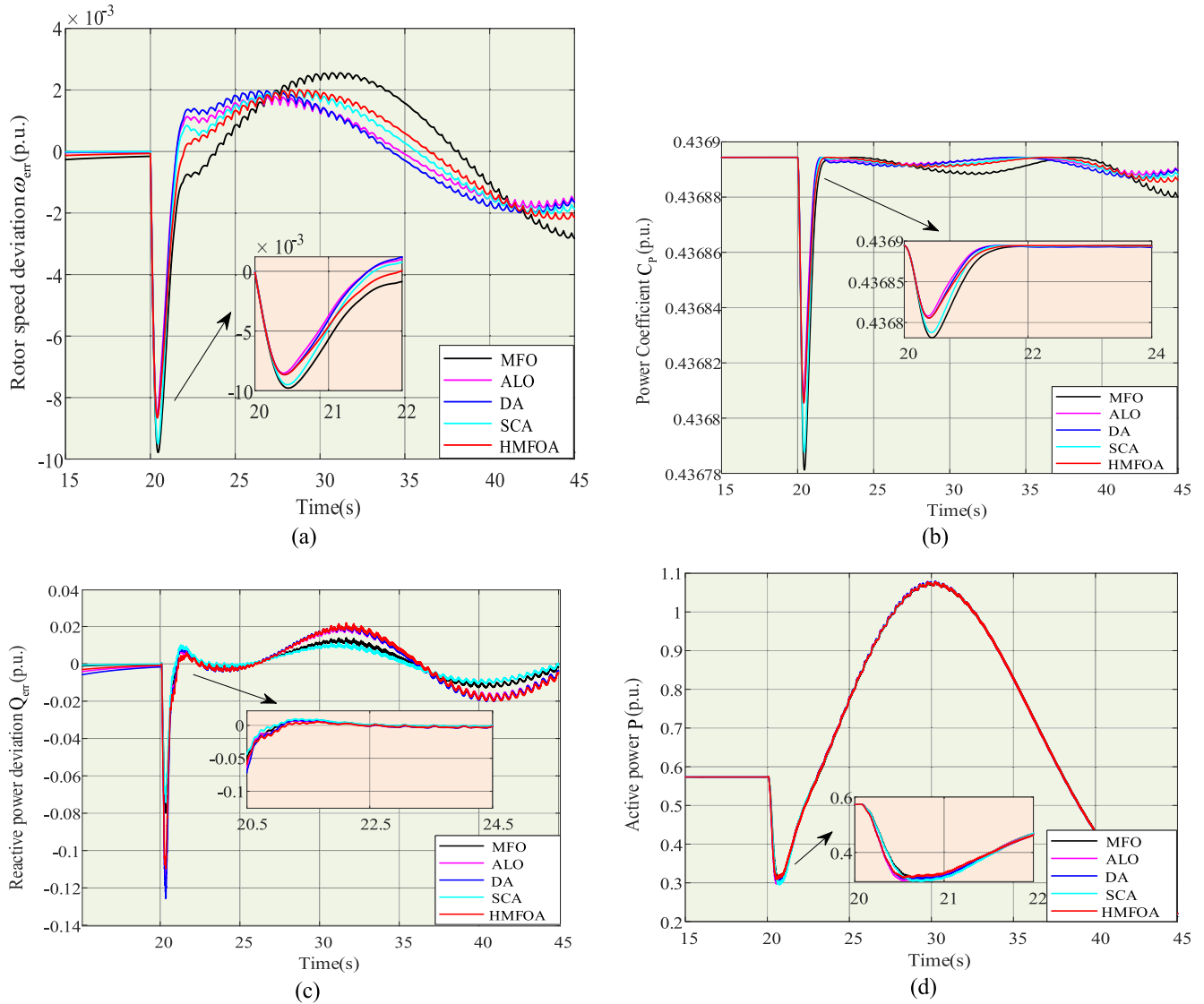
FIGURE 17. System response diagrams under gradual wind speed condition of Case II: (a) curves of rotor speed deviation; (b) curves of power coefficient; (c) curves of reactive power deviation; (d) curves of active power.

TABLE 8. Control parameters of high-dimensional multiple fractional-order optimization algorithm.

Symbols	K_{Q1}	K_{Q2}	K_{Q3}	K_{Q4}	α_{Q1}	α_{Q2}	α_{Q3}	α_{Q4}
Value	-0.17147	0.60184	0.18955	0.01567	-7.20×10⁻⁵	0.00531	0.00053	0.00016
Symbols	K_{Id1}	K_{Id2}	K_{Id3}	K_{Id4}	α_{Id1}	α_{Id2}	α_{Id3}	α_{Id4}
Value	0.09877	-0.00075	0.00728	-0.00139	0.17812	-0.00233	-0.00084	-0.00012
Symbols	K_{or1}	K_{or2}	K_{or3}	K_{or4}	α_{or1}	α_{or2}	α_{or3}	α_{or4}
Value	26.99426	95.10296	15.27172	32.62973	-0.00065	0.01515	0.00166	-0.00312
Symbols	K_{Iq1}	K_{Iq2}	K_{Iq3}	K_{Iq4}	α_{Iq1}	α_{Iq2}	α_{Iq3}	α_{Iq4}
Value	0.06240	0.00181	-1.18×10⁻⁵	-4.64×10⁻⁶	0.35749	-0.00086	-1.11×10⁻⁵	0.00407

TABLE 9. Statistical data after ten runs obtained by five intelligent optimization algorithms.

Algorithm	T	Execution time（hours）			Objective function				
		Max	Min	Mean	Worse	Best	Mean	Std. Dev.	Rel. Std. Dev.
MFO	200	20.5105	17.7565	19.0964	0.5784	0.5184	0.5486	0.0161	0.0293
ALO	200	19.9322	15.2563	16.7487	0.4750	0.4339	0.4503	0.0129	0.0286
DA	200	22.8060	12.3336	14.5750	0.4736	0.4469	0.4533	0.0103	0.0226
SCA	200	18.8037	14.7590	16.9632	0.5722	0.4144	0.5059	0.0771	0.1524
HMFOA	200	16.6941	13.8909	15.5401	0.4160	0.4107	0.4135	0.0024	0.0059

Std. Dev.=Standard deviation
Rel. Std. Dev.=Relative standard deviation

exploration ability, and the fractional-order differential direction has a strong exploitation ability.

2) The HMFOA is employed to the test of the baseline function against the other 18 optimization algorithms. The simulation results show the fitness function values, box-and-whisker plots of the fitness function, search trajectory of

search agents, convergence curve, and average fitness function curve. The simulation results show that the HMFOA has efficient optimization, stability of operation, extensive exploration ability, and high precision exploitation ability.

In all the case studies, the product factor of the proportional operator k_1 sets to $[-1, 1]$; the product factor of fractional-order integral operator k_2 sets to $[-1, 1]$; the product factor of fractional-order differential operator k_2 sets to
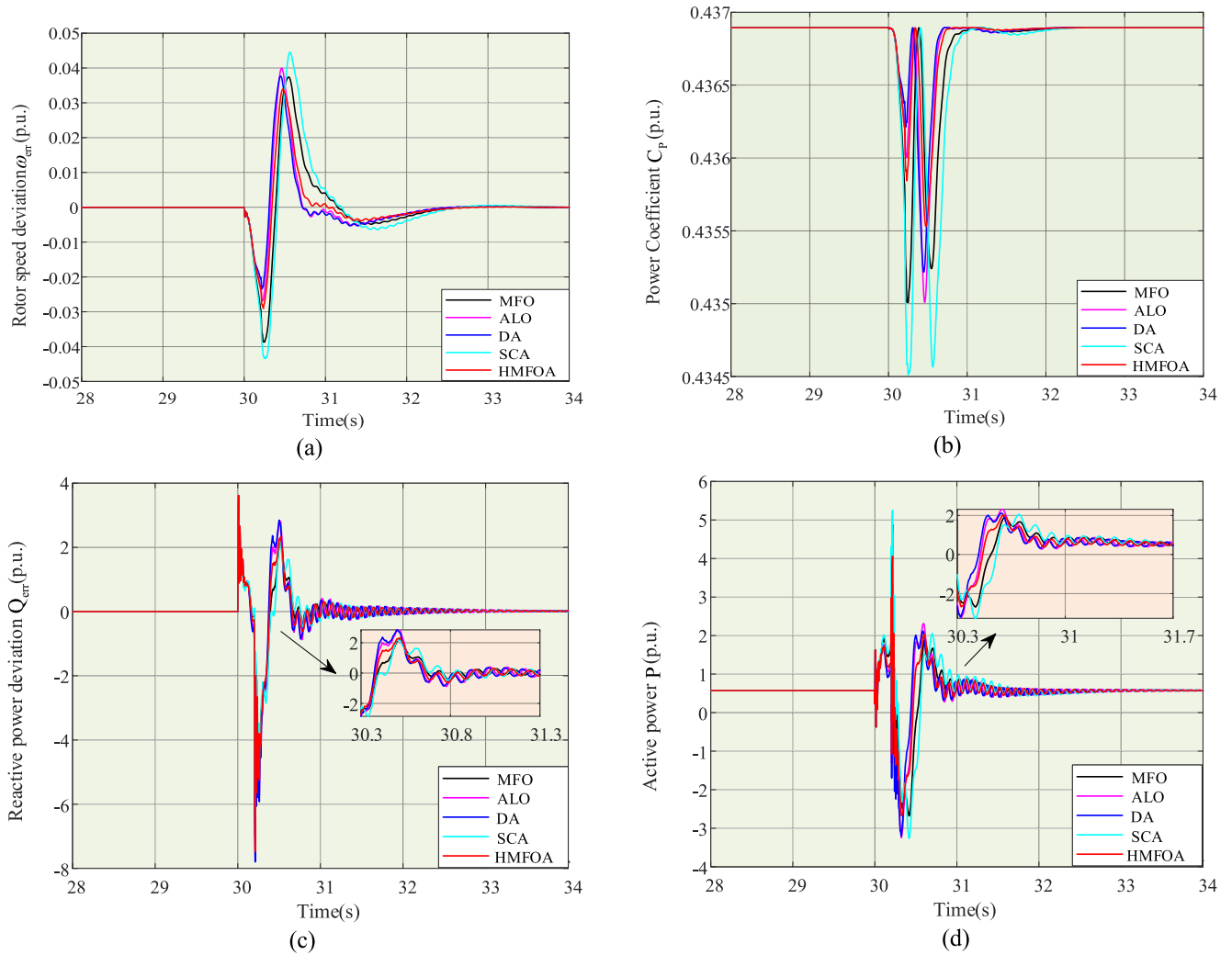
FIGURE 18. Response curves of Case II: (a) Werr curves; (b) Cp curves; (c) Qerr curves; (d) P curves.

[−1, 1]; the fractional-order integral order φ sets to [1,1.5]; the fractional-order differential order δ sets to [0.5, 1].

According to the theory that there is no free lunch, there is no method that can obtain the optimal solution quickly and accurately in any complex engineering scenario. In addition, the HMFOA proposed in this study is particularly applicable to the parameter optimization problem of optimizing complex controllers for HDMFOC. The HMFOA proposed in this study is more complex than PID. In addition, the running time of HMFOA is longer than that of PID. Besides, HMFOA is not suitable for the optimization of deep reinforcement learning and reinforcement learning algorithms. Instead, HMFOA is only appropriate for the optimization of traditional PID and HDMFOC controllers. The HMFOA proposed in this study is particularly suitable for the optimization problem of the parameters of traditional control algorithms containing fractional-order or proportional-integral differentiation, while it is not suitable for the optimization problem of complex control algorithms. In particular, this study applies the

idea of controllers to optimization algorithms, which is a slightly difficult scientific problem to understand.

V. CONCLUSION

This paper presents an HMFOA based on HDMFOA, which is applied to tune the parameters of HDMFOA of the RSC in the DFIG. The major contributions are summarized below.

1) The HMFOA has three search directions, namely, proportional direction, fractional-order integral direction, and fractional-order differential direction, which can balance exploration and exploitation in the whole. The exploration ability of fractional-order integral direction is high, improving the global search range; the exploitation ability of fractional-order differential direction is strong, improving the accuracy of local optimal solution search.

2) In the simulation results, HMFOA is verified to have excellent optimization capability on single-objective optimization problems.

3) The HMFOA is applied to the parameter tuning of the RSC in the DFIG-based wind energy systems. The simulation results prove the feasibility and reliability of the HMFOA for wind energy systems.

In the future works, i) consider a more comprehensive range of wind speed changes, more essential constraints, and dynamic performance indicators to meet the increasing practical needs of engineering applications; ii) consider the applications of the HMFOA to the controllers of grid-side converters of power systems; iii) consider the application of the HMFOA to the MPPT of permanent magnet synchronous generators and photovoltaic power generations.

VI. COMPLIANCE WITH ETHICAL STANDARDS
Conflict of Interest: The authors declare that they have no conflict of interest.

Ethical approval: This article does not contain any studies with human participants or animals performed by any of the authors.

REFERENCES

[1] Y. Xiang, L. Zhou, Y. Huang, X. Zhang, Y. Liu, and J. Liu, "Reactive coordinated optimal operation of distributed wind generation," *Energy*, vol. 218, Mar. 2021, Art. no. 119417.

[2] E. P. P. Soares-Ramos, L. de Oliveira-Assis, R. Sarrias-Mena, and L. M. Fernández-Ramírez, "Current status and future trends of offshore wind power in Europe," *Energy*, vol. 202, Jul. 2020, Art. no. 117787.

[3] K.-H. Lu, C.-M. Hong, and Q. Xu, "Recurrent wavelet-based Elman neural network with modified gravitational search algorithm control for integrated offshore wind and wave power generation systems," *Energy*, vol. 170, pp. 40–52, Mar. 2019.

[4] A. Mishra, P. M. Tripathi, and K. Chatterjee, "A review of harmonic elimination techniques in grid connected doubly fed induction generator based wind energy system," *Renew. Sustain. Energy Rev.*, vol. 89, pp. 1–15, Jun. 2018.

[5] Y. Xu, H. Nian, T. Wang, L. Chen, and T. Zheng, "Frequency coupling characteristic modeling and stability analysis of doubly fed induction generator," *IEEE Trans. Energy Convers.*, vol. 33, no. 3, pp. 1475–1486, Sep. 2018.

[6] A. Kadri, H. Marzougui, A. Aouiti, and F. Bacha, "Energy management and control strategy for a DFIG wind turbine/fuel cell hybrid system with super capacitor storage system," *Energy*, vol. 192, Feb. 2020, Art. no. 116518.

[7] F. Mazouz, S. Belkacem, I. Colak, S. Drid, and Y. Harbouche, "Adaptive direct power control for double fed induction generator used in wind turbine," *Int. J. Electr. Power Energy Syst.*, vol. 114, Jan. 2020, Art. no. 105395.

[8] S. Gao, H. Zhao, Y. Gui, D. Zhou, V. Terzija, and F. Blaabjerg, "A novel direct power control for DFIG with parallel compensator under unbalanced grid condition," *IEEE Trans. Ind. Electron.*, vol. 68, no. 10, pp. 9607–9618, Oct. 2021.

[9] M. R. A. Kashkooli, S. M. Madani, and T. A. Lipo, "Improved direct torque control for a DFIG under symmetrical voltage dip with transient flux damping," *IEEE Trans. Ind. Electron.*, vol. 67, no. 1, pp. 28–37, Jan. 2020.

[10] W. Ayrir, M. Ourahou, B. El Hassouni, and A. Haddi, "Direct torque control improvement of a variable speed DFIG based on a fuzzy inference system," *Math. Comput. Simul.*, vol. 167, pp. 308–324, Jan. 2020.

[11] B. Yang, X. Zhang, T. Yu, H. Shu, and Z. Fang, "Grouped grey wolf optimizer for maximum power point tracking of doubly-fed induction generator based wind turbine," *Energy Convers. Manage.*, vol. 133, pp. 427–443, Feb. 2017.

[12] J. Chen, W. Zhang, B. Chen, and Y. Ma, "Improved vector control of brushless doubly fed induction generator under unbalanced grid conditions for offshore wind power generation," *IEEE Trans. Energy Convers.*, vol. 31, no. 1, pp. 293–302, Mar. 2016.

[13] H. Jenkal, B. Bossoufi, A. Boulezhar, A. Lilane, and S. Hariss, "Vector control of a doubly fed induction generator wind turbine," *Mater. Today, Proc.*, vol. 30, pp. 976–980, 2020.

[14] B. Kelkoul and A. Boumediene, "Stability analysis and study between classical sliding mode control (SMC) and super twisting algorithm (STA) for doubly fed induction generator (DFIG) under wind turbine," *Energy*, vol. 214, Jan. 2021, Art. no. 118871.

[15] M. Abolvafaei and S. Ganjefar, "Maximum power extraction from fractional order doubly fed induction generator based wind turbines using homotopy singular perturbation method," *Int. J. Electr. Power Energy Syst.*, vol. 119, Jul. 2020, Art. no. 105889.

[16] J. Wang, D. Bo, Q. Miao, Z. Li, X. Wu, and D. Lv, "Maximum power point tracking control for a doubly fed induction generator wind energy conversion system based on multivariable adaptive super-twisting approach," *Int. J. Electr. Power Energy Syst.*, vol. 124, Jan. 2021, Art. no. 106347.

[17] L. Yin and Q. Gao, "Proportional–integral–derivative optimization algorithm for double-fed induction generator with the maximum wind power tracking technique," *Soft Comput.*, vol. 25, no. 4, pp. 3097–3111, Feb. 2021.

[18] L. Yin and Q. Gao, "Multi-objective proportional–integral–derivative optimization algorithm for parameters optimization of double-fed induction generator-based wind turbines," *Appl. Soft Comput.*, vol. 110, Oct. 2021, Art. no. 107673.

[19] Z. Tian, "Backtracking search optimization algorithm-based least square support vector machine and its applications," *Eng. Appl. Artif. Intell.*, vol. 94, Sep. 2020, Art. no. 103801.

[20] D. H. Kim, "Hybrid GA-BF based intelligent PID controller tuning for AVR system," *Appl. Soft Comput.*, vol. 11, no. 1, pp. 11–22, Jan. 2011.

[21] W. Deng, J. Xu, Y. Song, and H. Zhao, "Differential evolution algorithm with wavelet basis function and optimal mutation strategy for complex optimization problem," *Appl. Soft Comput.*, vol. 100, Mar. 2021, Art. no. 106724.

[22] X. Zhang, Q. Kang, and X. Wang, "Hybrid biogeography-based optimization with shuffled frog leaping algorithm and its application to minimum spanning tree problems," *Swarm Evol. Comput.*, vol. 49, pp. 245–265, Sep. 2019.

[23] M. Singh, R. N. Patel, and D. D. Neema, "Robust tuning of excitation controller for stability enhancement using multi-objective metaheuristic firefly algorithm," *Swarm Evol. Comput.*, vol. 44, pp. 136–147, Feb. 2019.

[24] A. Saxena, R. Kumar, and S. Das, "β-chaotic map enabled grey wolf optimizer," *Appl. Soft Comput.*, vol. 75, pp. 84–105, Feb. 2019.

[25] M. J. Blondin, J. Sanchis, P. Sicard, and J. M. Herrero, "New optimal controller tuning method for an AVR system using a simplified ant colony optimization with a new constrained Nelder–Mead algorithm," *Appl. Soft Comput.*, vol. 62, pp. 216–229, Jan. 2018.

[26] M. A. Ebrahim, M. Becherif, and A. Y. Abdelaziz, "Dynamic performance enhancement for wind energy conversion system using moth-flame optimization based blade pitch controller," *Sustain. Energy Technol. Assessments*, vol. 27, pp. 206–212, Jun. 2018.

[27] A. Saad, S. A. Khan, and A. Mahmood, "A multi-objective evolutionary artificial bee colony algorithm for optimizing network topology design," *Swarm Evol. Comput.*, vol. 38, pp. 187–201, Feb. 2018.

[28] A. K. Ball, S. S. Roy, D. R. Kisku, N. C. Murmu, and L. D. S. Coelho, "Optimization of drop ejection frequency in EHD inkjet printing system using an improved firefly algorithm," *Appl. Soft Comput.*, vol. 94, Sep. 2020, Art. no. 106438.

[29] H. Faris, M. A. Hassonah, A. M. Al-Zoubi, S. Mirjalili, and I. Aljarah, "A multi-verse optimizer approach for feature selection and optimizing SVM parameters based on a robust system architecture," *Neural Comput. Appl.*, vol. 30, no. 8, pp. 2355–2369, Oct. 2018.

[30] E. Y. Bejarbaneh, A. Bagheri, B. Y. Bejarbaneh, S. Buyamin, and S. N. Chegini, "A new adjusting technique for PID type fuzzy logic controller using PSOSCALF optimization algorithm," *Appl. Soft Comput.*, vol. 85, Dec. 2019, Art. no. 105822.

[31] D. H. Wolpert and W. G. Macready, "No free lunch theorems for optimization," *IEEE Trans. Evol. Comput.*, vol. 1, no. 1, pp. 67–82, Apr. 1997.

[32] Q. Zhu, M. Xu, W. Liu, and M. Zheng, "A state of charge estimation method for lithium-ion batteries based on fractional order adaptive extended Kalman filter," *Energy*, vol. 187, Nov. 2019, Art. no. 115880.

[33] T. A. A. Ali, Z. Xiao, S. Mirjalili, and V. Havyarimana, "Efficient design of wideband digital fractional order differentiators and integrators using multi-verse optimizer," *Appl. Soft Comput.*, vol. 93, Aug. 2020, Art. no. 106340.

[34] M. Al-Dhaifallah, A. M. Nassef, H. Rezk, and K. S. Nisar, "Optimal parameter design of fractional order control based INC-MPPT for PV system," *Sol. Energy*, vol. 159, pp. 650–664, Jan. 2018.

[35] L. Yin, X. Cao, and L. Chen, "High-dimensional multiple fractional order controller for automatic generation control and automatic voltage regulation," *Int. J. Control, Autom. Syst.*, vol. 20, no. 12, pp. 3979–3995, Dec. 2022.

[36] S. Mirjalili, "SCA: A sine cosine algorithm for solving optimization problems," *Knowl.-Based Syst.*, vol. 96, pp. 120–133, Mar. 2016.

[37] O. Soares, H. Gonçalves, A. Martins, and A. Carvalho, "Nonlinear control of the doubly-fed induction generator in wind power systems," *Renew. Energy*, vol. 35, no. 8, pp. 1662–1670, Aug. 2010.

[38] B. Yang, T. Yu, H. Shu, J. Dong, and L. Jiang, "Robust sliding-mode control of wind energy conversion systems for optimal power extraction via nonlinear perturbation observers," *Appl. Energy*, vol. 210, pp. 711–723, Jan. 2018.

[39] L. Yin, X. Cao, and S. Wang, "Deep learning-accelerated optimization algorithm for controller parameters optimization of doubly-fed induction generators," *Appl. Soft Comput.*, vol. 131, Dec. 2022, Art. no. 109800.

[40] F. Mei and B. Pal, "Modal analysis of grid-connected doubly fed induction generators," *IEEE Trans. Energy Convers.*, vol. 22, no. 3, pp. 728–736, Sep. 2007.

JIANBO QIN was born in Guangxi, China, in 1983. He received the B.S. degree in automation in China, in 2006, the M.S. degree in control theory and control engineering in China, in 2009, and the Ph.D. degree in electrical engineering in China, in 2022. His research interests include power system analysis and control, and torsional vibrations analysis and control.

XIAOZHE YANG received the B.S. and M.S. degrees from the Guilin University of Electronic Technology, Guangxi, China, in 2011 and 2015, respectively. He is currently a Computer Technology Engineer with Nanning University, Guangxi. His research interests include computer vision, object recognition, and few-shot learning.

LINFEI YIN was born in Jiujiang, Jiangxi, China, in 1990. He received the B.S. and M.S. degrees in information engineering from Nanchang Hangkong University, Nanchang, China, in 2012 and 2015, respectively, and the Ph.D. degree from the College of Electric Power Engineering, South China University of Technology, Guangzhou, China, in 2018. He is currently an Associate Professor with the College of Electrical Engineering, Guangxi University, Nanning, Guangxi, China. His major research interest includes artificial intelligence techniques in the operation of power systems.

XINGHUA TAO received the B.S. and M.S. degrees from the Naval University of Engineering, Hubei, China, in 1994 and 2002, respectively, and Ph.D. degree from Tsinghua University, in 2011. He is currently an Associate Professor with Nanning University, Guangxi. His research interests include power electronics, motor control, and power system control.

NAN MO was born in Lipu, Guangxi, China, in 1999. He received the B.S. degree in automation from the Shanghai Institute of Technology, Shanghai, China, in 2022. He is currently pursuing the M.S. degree with the College of Electrical Engineering, Guangxi University, Nanning, Guangxi. His major research interest includes artificial intelligence techniques in the operation of power systems.

LIKUN HU received the B.Sc. and M.S. degrees from the Harbin University of Science and Technology, Harbin, China, in 1999 and 2002, respectively, and the Ph.D. degree from the Harbin Institute of Technology, Harbin, in 2008. He is currently a Professor with Guangxi University, Nanning, China. His main research interests include robot dynamics and control, robot motion planning, robot vision, and environment perception.

• • •